Available online at www.sciencedirect.com
ScienceDirect
Medical Image Analysis 11 (2007) 282–301
MEDICAL IMAGE ANALYSIS
www.elsevier.com/locate/media

Predicting soft tissue deformations for a maxillofacial surgery planning system: From computational strategies to a complete clinical validation

W. Mollemans [a,*], F. Schutyser [a], N. Nadjmi [b], F. Maes [a], P. Suetens [a]

[a] *Medical Image Computing (Radiology – ESAT/PSI), Faculties of Medicine and Engineering, University Hospital Gasthuisberg, Herestraat 49, B-3000 Leuven, Belgium*
[b] *Eeuwfeestkliniek, Harmoniestraat 68, B-2018 Antwerpen, Belgium*

Received 3 February 2006; received in revised form 3 August 2006; accepted 15 February 2007
Available online 19 March 2007

Abstract

In the field of maxillofacial surgery, there is a huge demand from surgeons to be able to pre-operatively predict the new facial outlook after surgery. Besides the big interest for the surgeon during the planning, it is also an essential tool to improve the communication between the surgeon and his patient. In this work, we compare the usage of four different computational strategies to predict this new facial outlook. These four strategies are: a linear Finite Element Model (FEM), a non-linear Finite Element Model (NFEM), a Mass Spring Model (MSM) and a novel Mass Tensor Model (MTM). For true validation of these four models we acquired a data set of 10 patients who underwent maxillofacial surgery, including pre-operative and post-operative CT data. For all patient data we compared in a quantitative validation the predicted facial outlook, obtained with one of the four computational models, with post-operative image data. During this quantitative validation distance measurements between corresponding points of the predicted and the actual post-operative facial skin surface, are quantified and visualised in 3D. Our results show that the MTM and linear FEM predictions achieve the highest accuracy. For these models the average median distance measures only 0.60 mm and even the average 90% percentile stays below 1.5 mm. Furthermore, the MTM turned out to be the fastest model, with an average simulation time of only 10 s. Besides this quantitative validation, a qualitative validation study was carried out by eight maxillofacial surgeons, who scored the visualised predicted facial appearance by means of pre-defined statements. This study confirmed the positive results of the quantitative study, so we can conclude that fast and accurate predictions of the post-operative facial outcome are possible. Therefore, the usage of a maxillofacial soft tissue prediction system is relevant and suitable for daily clinical practice.

Keywords: Maxillofacial surgery; Soft tissue simulation; Therapy planning; Mass Tensor Model

1. Introduction

1.1. Background

Maxillofacial surgery treats abnormalities of the skeleton of the head. Skull remodelling implies osteotomies, bone fragment repositioning, restoration of bone defects and inserting implants. Since the human face plays a key role in interpersonal relationships, people are very sensitive to changes to their outlook. Even very subtle malformations of facial proportions can strongly affect the appearance of a face (Farkas, 1994). Therefore, planning of the operation and reliable prediction of the facial changes are very important in view of a better preparation, an improved surgical outcome and shorter operation time.

Traditional computer-aided maxillofacial planning systems start from 2D lateral X-rays. In these planning environments, the surgeon can define an appropriate

* Corresponding author. Tel.: +32 16349032; fax: +32 16349001.
E-mail address: wouter.mollemans@uz.kuleuven.ac.be (W. Mollemans).

1361-8415/$ - see front matter © 2007 Elsevier B.V. All rights reserved.
doi:10.1016/j.media.2007.02.003

osteotomy line and derive the necessary displacement of each bone segment. Besides this bone-related planning, most commercial 2D cephalometric planning systems nowadays allow to analyse the facial profile of the patient and to do some sort of video overlaying (Smith et al., 2004; Cousley et al., 2003). As such it becomes possible to give a first impression of the patient's expected post-operative outlook. Notwithstanding the better preparation of the surgeon and improved communication between surgeon and patient thanks to these 2D planning systems, these systems cannot define the full 3D transformation of the bone parts. Especially for patients suffering from dysmorphosis both in the coronal and sagittal planes, these 2D systems which rely on only 2D lateral images are insufficient. Moreover, they demand from the surgeon good mental work and when communicating with the patient, they are limited to only lateral views of the patient's expected post-operative appearance.

Since the introduction of computed tomography in 1972 it became possible to acquire true 3D anatomical information for every patient. The development of 3D visualisation techniques in the late eighties, like the marching cubes algorithm (Lorensen and Cline, 1987), pushed the development of applications that used computer generated anatomical models. Soon the first craniofacial planning systems were born (Burk et al., 1986). These first 3D computer aided planning systems made it possible to inspect the patient's skull and perform simple osteotomies in a 3D simulation environment. More advanced planning systems that allow complete manipulation of bone parts, were developed in the late nineties (Everett et al., 2000; Zachow et al., 2001). In 2000, Schutyser et al. (2000) reported on a 3D image-based planning system which includes osteotomy simulation with user-defined cutting trajectories, virtual distraction employing specific biomechanical models and evaluation tools based on a cephalometric reference frame. According to the surgeon's findings, different choices could be virtually redone in this environment in order to optimise the therapy. However, because of the high impact of maxillofacial therapy on the patient's face, not only this bone-related pre-operative planning of the surgery, but also the prediction of the deformation of the soft tissues became highly desirable.

1.2. 3D soft tissue modelling: state of the art

The idea of predicting the new patient's facial outlook with a computer aided maxillofacial planning system, was originally introduced by Vannier et al. (1983). At that moment, especially the computer animation world was expertised in facial modelling. Most of these facial modellers represented the face as a collection of regularly assembled mass-spring entities and were mainly focused on real-time output and realistic graphical behaviour (Terzopoulos and Walters, 1990; Lee et al., 1995).

The first maxillofacial soft tissue prediction systems, were strongly inspired by these computer graphics facial modellers. Koch et al. (1996) presented a non-linear finite-element approach to simulate the new facial outlook which provides a C^1-continuous finite element surface. Linear springs were used to connect the facial surface with the underlying bone structures. He applied virtual maxillofacial interventions on the Visible Human Data Set (Ackermann, 1998) and qualitatively validated the new predicted facial outlook by visual inspection. Afterwards Keeve et al. (1998) compared the two most popular soft tissue models for maxillofacial surgery, namely the Mass Spring Model, that originated from the computer animation world and the Finite Element Model, that was assumed to be a more biomechanical relevant model. His comparison was based on a qualitative visual inspection of the predicted facial outlooks calculated with each model. He concluded that although the Mass Spring Model could never be biomechanically correct, the speed and the easy architecture of this model could be a serious advantage over the more accurate but computationally intensive Finite Element Model. At the same moment, Sarti et al. (1999) presented a volumetric Finite Element Model applied on a cubic grid that coincide with the voxel grid of the CT data. This voxel-based modelling is advantageous from an image processing point of view (the data remains available on a voxel grid), but demands a large number of finite elements which is memory expensive. He implemented his model on a super computer and achieved good simulation results.

Despite these good results, it became clear that planning systems running on special designed computers, would never be accepted in daily clinical practice. Moreover, as already suggested for 2D soft tissue profile planning systems (Smith et al., 2004; Cousley et al., 2003), it is important to also incorporate the changes in facial outlook during planning. The bone-related planning should be adjusted in function of the new predicted facial outlook which implies that the soft tissue prediction step needs to become part of the complete treatment planning. Therefore, it is necessary that predictions are calculated in a fast and accurate way. The speed in which the new facial outlook could be calculated, became a new goal in the search of a good computer aided maxillofacial planning system.

Also in other research fields, researchers tried to simulate accurately the deformation behaviour of soft tissues and tried to find a golden mean between accuracy and speed. Especially for surgical simulators used for training, where real-time simulations have to be performed, this trade-off became very clear. In this research area, a couple of novel computational strategies were presented (Bro-Nielsen and Cotin, 1996; Cotin et al., 1999; Picinbono et al., 2003) in order to tackle this trade-off. More recent maxillofacial soft tissue planning systems were strongly inspired by these novel models.

Zachow et al. (2000) presented a tetrahedral volumetric FEM model. These tetrahedral elements, which have less degrees of freedom than the prismatic elements that were

often used before, are assumed to be better suited for simulation of the deformation of biological objects. By making a trade-off between the number of elements and the accuracy of the model, he was able to compute the new facial outlook of a real patient in less than 5 min. He noted that thanks to these short calculation times his model became appropriate for use in daily clinical practice. Two years later Teschner (2001) and Meehan et al. (2003) reported on a multi-layer non-linear Mass Spring Model. In his work, he introduced the combination of using a Mass Spring Model with a static constraint to calculate the soft tissue deformations. Until then Mass Spring Models were typically combined with a time-integration scheme of the Newtonian motion equation to find the deformation of the soft tissues. Teschner suggested that only the deformation of the tissues were important and not the animation from the original position to the new deformed position. Consequently, he proposed the use of an iterative scheme to directly find this new deformed position. By doing so and by lowering the number of mass points, he could reduce the simulation time of his Mass Spring Model to less than 20 s. He used the planning system to predict the new facial outlook of one real patient and compared qualitatively the prediction result and the real post-operative facial outlook. Other important work in the field of maxillofacial soft tissue prediction systems was realised by Chabanas et al. (2003). He was one of the first to present a complete maxillofacial planning system that incorporated the bone-related planning and the prediction of the new facial outlook. To overcome the difficult meshing step, he used a generic model that was elastically registered with patient specific data. A Finite Element solution was used to simulate the soft tissue deformation. The generic mesh contained 2284 mesh nodes and also muscle specific structures were incorporated in the mesh. This enabled not only prediction of the new facial outlook, but also simulation of the post-operative facial functional behaviour. This functional simulation of the facial expressions after surgery was introduced by Gladilin (2002) at the same moment.

More and more it became clear that before a maxillofacial soft tissue prediction system can be used in clinical practice, not only a qualitative validation of the predicted facial outlook is necessary, but also a real quantitative validation is required. Schutyser et al. (2000) noted as first that this quantitative validation should be a numerical comparison between the predicted and real post-operative facial skin surface. After first registering the predicted and actual post-operative facial skin surface based on an unaltered subspace, he quantified distances between both surfaces in 3D. Later, the relevance of this idea was confirmed by Chabanas et al. (2004). In this work, he quantitatively validated soft tissue predictions for three patients by measuring distances between the predicted facial surface and the real post-operative outcome. More recently, Zachow et al. (2004, 2005) reported on a quantitative validation for one relevant patient. He compared simulation results for different model parameters and concluded that a mean prediction error of 1–1.5 mm could be achieved with his model.

In previous work (Mollemans et al., 2003) we presented a Tetrahedral Mass Spring Model (MSM) to simulate based on a bone-related planning, the new facial appearance after a maxillofacial procedure. A tetrahedral model build-up was chosen to facilitate the meshing step compared to the multi-layered based models (Koch et al., 1996; Teschner, 2001) in which the meshing step, based on the approach of Waters (1992), is typically rather tedious and error-prone. Our MSM directly calculates the new facial outlook by solving static force constraint, as introduced by Teschner (2001). A major advantage of this model is the combination of a large number of elements, for a better accuracy, and a fast simulation time. We quantitatively validated our MSM by measuring distances between predicted and post-operative facial surface for three patients and concluded that pretty good results could be achieved with this model (Mollemans et al., 2004). Nevertheless, the usage of such a Tetrahedral MSM and MSM more generally, have some serious disadvantages, as discussed in Roose et al. (2005) and Mollemans et al. (2005). The most important drawback is that the MSM has no real bio-mechanical foundation.

1.3. Paper outline

This work mainly includes two parts. In the first part, we present four different computational strategies used to model the deformation behaviour of facial soft tissues for a maxillofacial planning system: a linear Finite Element Model (FEM), a non-linear FEM, a MSM and a Mass Tensor Model (MTM) (Cotin et al., 2000). This last model, MTM, was introduced by Cotin et al. (2000). Two extensions to the original model are introduced in order to adapt it for our specific application. The MTM has the easy architecture of the MSM but keeps the bio-mechanical relevance of FEM, moreover as shown it beats both other linear models in computation time.

In the second part of this text, we present a complete true validation work flow, including a quantitative and qualitative validation. Therefore, we acquired a data set of 10 patients containing for each patient pre-operative and post-operative CT data. After first introducing the qualitative and quantitative validation methods, results for each of the four computational strategies are presented and discussed.

Our results show that the MTM achieves the same accuracy as the linear FEM, but clearly beats MSM and the linear FEM in simulation time. No significant improvement of the simulation accuracy was found, when using the non-linear FEM. The validation study denotes moreover an acceptable error of the predictions for the MTM and linear FEM when quantitatively measuring distances between the predicted and real post-operative facial outlook. These positive results were confirmed by the qualitative validation

study, so that we are able to conclude that maxillofacial soft tissue prediction systems can be used in daily clinical practice.

2. Computational strategies for soft tissue modelling

Simulation of the deformation of the facial soft tissues due to bone movement, demands a mathematical model that is able to imitate the behaviour of the facial tissues. All approaches that have been proposed for this simulation, can be categorised in two main model types: Finite Element Models (FEM) and Mass Spring Models (MSM). Both methods have been investigated in our group in the past (Schutyser et al., 2000; Mollemans et al., 2003). In this section, we briefly summarize these two models and highlight the main benefits and disadvantages of both methods. Next, we introduce the Mass Tensor Model (MTM), as some sort of golden mean between both methods. Since one of the benefits of this MTM, compared to linear FEM or MSM, is the fast calculation time, we discuss this topic in more detail in the last part of this section.

2.1. Finite element model

To model the deformation behaviour of living soft tissues, we start from the mechanical equilibrium equations:

$$\begin{aligned}\frac{\partial\sigma_{xx}}{\partial x}+\frac{\partial\tau_{xy}}{\partial y}+\frac{\partial\tau_{xz}}{\partial z}+F_x&=0\\ \frac{\partial\tau_{xy}}{\partial x}+\frac{\partial\sigma_{yy}}{\partial y}+\frac{\partial\tau_{yz}}{\partial z}+F_y&=0\\ \frac{\partial\tau_{xz}}{\partial x}+\frac{\partial\tau_{yz}}{\partial y}+\frac{\partial\sigma_{zz}}{\partial z}+F_z&=0\end{aligned}\tag{1}$$

with σ_{xx}, σ_{yy}, σ_{zz}, τ_{xy}, τ_{xz} and τ_{yz} the stress components and $\mathbf{F}(F_x,F_y,F_z)$ the volume forces. The material properties (Fung, 1993) are introduced into these equations through the constitutive equations relating stresses and strains. Following the approach of Schutyser et al. (2000), the soft tissue can be modelled as a homogeneous, linear and elastic material, such that we can use Hooke's law:

$$\begin{bmatrix}\sigma_{xx}\\ \sigma_{yy}\\ \sigma_{zz}\\ \tau_{xy}\\ \tau_{yz}\\ \tau_{zx}\end{bmatrix}=\frac{E}{(1+v)(1-2v)}\times\begin{bmatrix}1-v & v & v & 0 & 0 & 0\\ v & 1-v & v & 0 & 0 & 0\\ v & v & 1-v & 0 & 0 & 0\\ 0 & 0 & 0 & \frac{1-2v}{2} & 0 & 0\\ 0 & 0 & 0 & 0 & \frac{1-2v}{2} & 0\\ 0 & 0 & 0 & 0 & 0 & \frac{1-2v}{2}\end{bmatrix}\begin{bmatrix}\epsilon_{xx}\\ \epsilon_{yy}\\ \epsilon_{zz}\\ \gamma_{xy}\\ \gamma_{yz}\\ \gamma_{zx}\end{bmatrix}$$
$$\Longleftrightarrow\boldsymbol{\sigma}=\mathbf{D}\boldsymbol{\epsilon}\tag{2}$$

with strain components ϵ_{xx}, ϵ_{yy}, ϵ_{zz}, γ_{xy}, γ_{xz}, γ_{yz}, Young's modulus E and Poisson coefficient v. If we define $\{\mathbf{X}\}$ as the initial configuration at time t_0 and $\mathbf{x}=\mathbf{x}(\mathbf{X},t)$ as the description of the point $\mathbf{X}$ at time t, the displacement vector $\mathbf{u}$ can be defined as $\mathbf{x}=\mathbf{X}+\mathbf{u}$. The Green Lagrange strain tensor relates the strains $\boldsymbol{\epsilon}$ to the displacement vector $\mathbf{u}$: $\boldsymbol{\epsilon}=\frac{1}{2}(\nabla\mathbf{u}+\nabla\mathbf{u}^{\mathrm{T}}+\nabla\mathbf{u}^{\mathrm{T}}\nabla\mathbf{u})$. When assuming that displacements are relatively small the last term of this tensor can be neglected resulting in the linearised Green Lagrange strain tensor: $\boldsymbol{\epsilon}=\frac{1}{2}(\nabla\mathbf{u}+\nabla\mathbf{u}^{\mathrm{T}})$. In a large deformation set-up, the full Green Lagrange tensor will be solved.

These equations are discretized using a 3D finite element method, resulting in a linear FEM when the linearised Green Lagrange tensor is solved or a non-linear FEM when solving the complete tensor. The continuum is modelled as a tetrahedral mesh. For the interpolation between the mesh nodes we use a basic linear, C_0 continuous shape function using four nodes for each tetrahedron (Zienkiewicz and Taylor, 2000).

For the linear FEM, the partial differential equations are reduced to a set of linear equations for the vertices of the tetrahedron mesh: $\mathbf{KU}=\mathbf{R}$ with $\mathbf{K}$ the global stiffness matrix for the entire model and $\mathbf{U}$ and $\mathbf{R}$ the displacement and elastic force acting in each mesh node, respectively. By defining a fixed displacement for a set of mesh nodes and demanding that in rest the total force in all other mesh nodes should be zero, the displacement of all mesh nodes can be found by solving the linear equations $\mathbf{KU}=\mathbf{R}$. To solve the finite element equations in a fast way we use a Jacobi preconditioned Krylov subspace method, namely GMRES (general minimum residual) (Saad and Schultz, 1986).

For the non-linear FEM, we use a commercial finite element analysis software package named CalculiX CrunchiX (Dhondt, 2004), which is available under the terms of the GNU General Public License. The non-linear equations were solved iteratively using an Incomplete Cholesky preconditioning (Kershaw, 1978).

FEM is a general discretization procedure of continuum problems posed by mathematically defined statements. As a consequence, this model has a very strong biomechanical relevance and is expected to be a very accurate model when simulating deformations of living tissues. These two properties make FEM an excellent choice from an accuracy point of view. Nonetheless, it is known that FEM has a high computational cost and large memory usage, which could result in rather long simulation times and may hamper application of this approach in daily clinical practice as already argued in the introduction. FEM extensions based on pre-computing the matrix system, have been presented in order to improve the online simulation time (Cotin et al., 1999). These extensions demand however a rather long pre-computation step.

2.2. Tetrahedral Mass Spring Model

A Mass Spring Model assumes a discretization of the deformable object into n mass points and a set of m con-

nections between each of these n mass points. For this we start from a tetrahedral discretization and assign a mass point to each mesh node and define a linear spring for each mesh edge. These linear springs follow Hooke's law:

$$F_s = k_s \triangle L \tag{3}$$

with F_s the magnitude of the elastic force working in the end points of the linear spring, k_s the linear spring constant and $\triangle L$ the difference between the rest length and the actual length of the spring.

In our model, we distinguish two types of points: join points and free points (see also Section 3.3). During simulation a well known displacement is applied to each of the join points, while the displacement of each free point is found by demanding that the total internal force $\mathbf{F}_i^{\text{int}}$ in each free point should be zero when the deformable model is in rest. The total internal force $\mathbf{F}_i^{\text{int}}$ of a free mass point i is given by

$$\mathbf{F}_i^{\text{int}} = \sum_{\forall \mathbf{p}_j \in S_i} k_j (\|\mathbf{p}_j - \mathbf{p}_i\| - L_j^0) \frac{\mathbf{p}_j - \mathbf{p}_i}{\|\mathbf{p}_j - \mathbf{p}_i\|} \tag{4}$$

with S_i denoting the set of springs connected to mass point i, $\mathbf{p}_f$ the 3D coordinates of point f, and L_j^0 and k_j the rest length and spring constant of spring j, respectively.

Demanding that the total internal force in each free point should be zero, is solved as an iterative minimisation problem with a steepest-gradient solution scheme. To reduce the calculation time a dynamic cut-out was implemented. In each iteration step there are a lot of points in which the resulting force is very small. Moreover forces working in point i at the start of iteration j can only have been changed in comparison to the previous iteration step when point i or a neighbouring point has been moved during iteration $j-1$. Consequently only points with an internal force larger than some threshold value should be considered in each iteration step and secondly, only points which are neighbours of a point that has been moved in the previous iteration, have to be evaluated in the next step.

Since we want to model the behaviour of facial soft tissues, we have to choose an appropriate value for the spring constants in order to meet the correct stress–strain relationship. Gelder (1998) suggested a formula to compute the spring stiffnesses for a 3D tetrahedral mesh that is closest to an elastic continuous representation. Let E be the material's Young's Modulus, then the spring constant of spring i is given by

$$k_i = \frac{E_i \sum_{\forall j \in \Omega_i} V_j}{(L_i^0)^2} \tag{5}$$

with Ω_i the collection of all tetrahedra containing spring i, V_j the volume of tetrahedron j and L_i^0 the rest length of spring i.

MSM finds its origin in the computer animation world (Keeve et al., 1998; Teschner, 2001). The very easy architecture and low memory usage make this model very attractive for fast simulators. However, our Tetrahedral MSM and MSM more generally have also some important disadvantages. Three important disadvantages are distinguished:

(1) In the Tetrahedral MSM an object is described into discrete mass points which are connected to each other by springs. A change of length of a spring induces a force in the direction of the spring. However, since no volume behaviour of the tetrahedron is incorporated, this may cause a possible 'flip over' of a spring (Roose et al., 2005).
(2) The value of the spring constant determines the elastic behaviour of the MSM. As shown in Bianchi et al. (2004) there should be some kind of topology dependent mapping of Young's Modulus to these spring constants. Although some suggestions are proposed of how this can be done (Bianchi et al., 2004; Gelder, 1998), the calculated value for the spring constant is only an approximation and has no true biomechanical relevance.
(3) In a MSM there is no way to really control the volume conservation during simulation, even when the model is extended with extra 'volume springs', as described in (Mollemans et al., 2003).

2.3. Mass Tensor Model

The fourth model introduced in this section, is a novel Mass Tensor Model (MTM) which can be seen as a mixture of FEM and MSM. On the one hand, the model preserves the easy architecture of the MSM and on the other hand the model has the bio-mechanical relevance of FEM.

2.3.1. The original model

The original MTM was introduced by Cotin et al. (2000) and Schwartz et al. (2005). In the MTM the modelled object is discretized into a tetrahedral mesh. Inside every tetrahedron T_i, the displacement field is defined by a linear interpolation of the displacement vectors of the four vertices of T_i, as defined by the finite element theory. The linear elastic energy of tetrahedron T_i can be expressed as a function of the displacements of the four vertices and of the two Lamé coefficients. These coefficients λ and μ are biomechanical elastic constants and directly proportional to the well-known material dependent Young's Modulus E and Poisson coefficient v, by the formula:

$$\lambda = \frac{vE}{(1+v)(1-2v)} \tag{6}$$

$$\mu = \frac{E}{2(1+v)} \tag{7}$$

The force applied at vertex j of tetrahedron T_i is defined as the derivative of the elastic energy of T_i:

$$\mathbf{F}_j^{T_i} = -\frac{\partial W_{\text{elastic}}(T_i)}{\partial \mathbf{p}_j} = \sum_{k=0}^{3} [\mathbf{K}_{jk}^{T_i}] \mathbf{u}_{T_i(k)} \tag{8}$$

with $\mathbf{p}_j$ the 3D coordinates of vertex j, $\mathbf{u}_{T_i(k)}$ the displacement of vertex k of tetrahedron T_i and $\mathbf{K}_{jk}^{T_i}$ the stiffness tensors for this tetrahedron. These tensors are completely determined by the initial position of each vertex of the tetrahedron and the Lamé coefficients, which are material specific. For details we refer to Cotin et al. (2000).

For the whole mesh, the total elastic force $\mathbf{F}_j$ at a vertex j is now simply the sum of the contributions of all tetrahedra containing this vertex j:

$$\mathbf{F}_j = \sum_{\forall T_i \in \Lambda_j} \mathbf{F}_j^{T_i} = \sum_{\forall T_i \in \Lambda_j} \sum_{k=0}^{3} [\mathbf{K}_{jk}^{T_i}] \mathbf{u}_{T_i(k)} \tag{9}$$

with Λ_j the collection of all tetrahedra adjacent to vertex j. This expression can be rewritten into the following simple form:

$$\begin{aligned} &\mathbf{F}_j = [\mathbf{K}_{jj}]\mathbf{u}_j + \sum_{\forall k \in \Psi_j} [\mathbf{K}_{jk}]\mathbf{u}_k \\ &\text{with } [\mathbf{K}_{jj}] = \sum_{\forall T_i \in \Lambda_j} [\mathbf{K}_{jj}^{T_i}] \quad \text{and} \quad [\mathbf{K}_{jk}] = \sum_{\forall T_i \in \Lambda_j} [\mathbf{K}_{jk}^{T_i}] \end{aligned} \tag{10}$$

with Ψ_j the collection of all mass points neighbouring to mass point j. This MTM results in an easy implementation with mass points and model tetrahedra and a straightforward way to evaluate the force in each mass point during simulation.

During simulation the displacement for a set of mass points is set fixed (the join points, see Section 3.3). The other model points (free points) will move due to elastic forces in these points induced by the displacement of these join points. The new rest position of these free points can than be found by time integrating the Newtonian motion equation (Cotin et al., 2000).

2.3.2. Extension 1: direct computation of the deformation

As already suggested in (Teschner, 2001; Mollemans et al., 2003) the usage of a time integration scheme, as mentioned above, can lead to slow convergence and errors in the estimation of the final position. In a maxillofacial surgery planning system the prediction of this final rest position is more important than the exact animation of the deformation. Therefore, we combined the original Mass Tensor Model with a static constraint to directly estimate the deformation without calculating the animation.

The new rest position is now found by demanding that in each free point the total elastic force should be zero when the object is in rest:

$$\mathbf{u}_j^{\text{new}} = \text{argmin} \|\mathbf{F}_j(\mathbf{u}_j)\| \quad \forall j \in \Gamma_{\text{free}} \tag{11}$$

with Γ_{free} the collection of all free mass points. To solve this optimisation problem, we use a local steepest gradient method which tries to minimise the total elastic force in each free point in every iteration step. So in iteration step p we get

$$\mathbf{F}_j(\mathbf{u}_j^p) = 0 \rightarrow \mathbf{u}_j^p = -[\mathbf{K}_{jj}]^{-1} \left(\sum_{\forall k \in \Psi_j} [\mathbf{K}_{jk}] \mathbf{u}_k^{p-1} \right) \tag{12}$$

Since all $[\mathbf{K}_{jj}]$ and $[\mathbf{K}_{jk}]$ are only dependent on the initial mesh configuration and the two biomechanical constants, λ and μ, we can pre-compute all $[\mathbf{K}_{jj}]^{-1}$ and $[\mathbf{K}_{jk}]$. Hence, the optimisation problem will be restricted to a series of matrix–vector multiplications and matrix summations.

2.3.3. Extension 2: a local dynamic stop criterion

A second improvement was introduced to the original MTM. Suppose we define a total elastic force threshold F_{thresh}. When the total elastic force $\|\mathbf{F}_j\|$ in each model point becomes smaller than this F_{thresh}, iterations will be stopped early. We name the difference between the predicted result when F_{thresh} is set to zero and the outcome when a non-zero value is assigned to F_{thresh}, the precision of the MTM. This definition of the term precision is consistent to the work of Hofer et al. (2005), where precision was defined as a measurement for the 'internal accuracy' of a model. It is needless to make this precision a lot higher than the achieved total accuracy, defined as the difference between the predicted outcome and the real post-operative new facial outlook. As a consequence iterations can be cut-off early, which will cause a serious gain in simulation time.

Defining a good overall value for F_{thresh} is however impossible, since this value will be dependent on the mesh topology and the biomechanical constants. Therefore, we propose to look to the mean gradient of the displacement field over a number of iterations, to determine when iterations should stop. If this gradient becomes very small in every model point, we can conclude that we must be close to the real solution and can ensure that the error made by the limited precision is negligible to the accuracy of the prediction. This dynamic stop criterion enables the combination of high accuracy with fast simulation times.

This threshold can be reached in different model points after a different number of performed iterations. Moreover, the elastic force in point j at the start of iteration k can only have been changed since iteration $k-1$ when point j or a neighbouring point has been moved during iteration $k-1$. Due to the easy architecture of the MTM, storing information locally in each mass point, these two criteria can easily be incorporated in the iterative solution scheme and will result in a shorter simulation time.

2.3.4. Validation of the local dynamic stop criterion

We validated the local dynamic stop criterion of the MTM in two ways. In the first section we try to clarify the effect on the accuracy of the stop criterion. In the second part we highlight the gain in simulation time when comparing to FEM or MSM simulations.

2.3.5. Precision of MTM

For validation we arbitrarily selected five patient CT data sets and constructed for each data set a tetrahedral mesh which encloses the facial soft tissues, as explained in Section 3.1. This tetrahedral mesh serves as input for our Tetrahedral Mass Tensor Model. For each patient boundary conditions, defining the join and free model

points, were generated based on a realistic bone-related planning (see Section 3.3). After applying these conditions to the model, the soft tissue deformations were calculated by searching the new rest position for each free model point, as described in Section 2.3.2. After each iteration step the new calculated position for each point was saved. Based on this saved data the maximal gradient of the displacement field and the minimal precision over all free model points were calculated during each iteration step. The precision of the prediction at iteration step n, was derived by measuring the distance between the final position, when the total elastic force is zero in each model point, and the position at iteration step n, for each model point. The graphs in Fig. 1 summarize the precision data for each of the five patients.

As will be discussed in Section 3, the mean accuracy of the Mass Tensor Model equals approximately 1.5 mm for this data set of five patients. When the minimal precision of our MTM becomes smaller than, for example, one-fifth of this mean accuracy (≈0.3 mm), we can suppose that precision becomes negligible compared to the accuracy of the prediction and that iterations can be cut-off. This cut-off boundary is indicated on each graph in Fig. 1 and summarized in Table 1.

Table 1 shows that when the minimal precision becomes smaller than 0.3 mm, the mean precision over all model points equals on average 0.039 mm. This very low mean value suggests that only a very small group of model points have not reached their final rest position yet. Moreover the distance between the current position of these points and their final rest position is small compared to the real accuracy of the prediction and will therefore not influence the final prediction accuracy. As a consequence iterations can be stopped early. We can derive from Table 1 that this boundary is reached when the maximal gradient of the displacement field becomes smaller than 0.001.

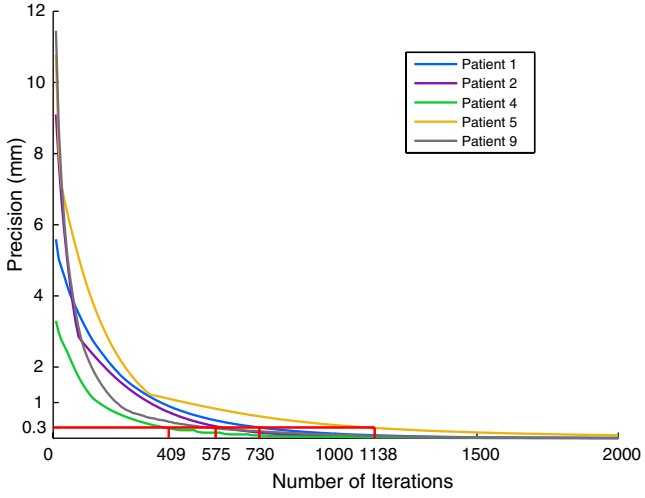

Fig. 1. The minimal precision in mm over all free model points after each iteration step for five arbitrarily chosen patient data sets. The red lines indicate when the minimal precision becomes smaller than 0.3 mm. (For interpretation of the references to color in this figure legend, the reader is referred to the web version of this article.)

Table 1
Table showing the number of performed iterations (N_{its}), the corresponding minimal (P_{min}) and mean precision (P_{mean}) of the current prediction and the maximal gradient (G_{max}) of the deformation field over all model points after n iterations

Patient	N_{its}	P_{min} (mm)	P_{mean} (mm)	G_{max}
1	727	0.30	0.058	0.0010
2	583	0.29	0.021	0.0015
3	409	0.28	0.065	0.0016
4	1138	0.28	0.011	0.0005
5	570	0.29	0.041	0.0017
Average	685.4	0.288	0.039	0.0012

2.3.6. Simulation time

To investigate in more detail the time gain due to the local stop criterion, we measured the time gain of the MTM compared to the linear FEM and MSM, in function of the numbers of tetrahedra used in the tetrahedral model. Therefore, we created a set of virtual test cubes having the same dimensions but containing a different number of tetrahedra. During simulation the centre of the cube was moved 6 mm upwards. Simulation times were recorded for each biomechanical model and results are summarized in Fig. 2.

These results reveal that the simulation time of FEM and MTM behaves more or less linear in function of the number of tetrahedra in our region of interest (30.000–200.000 tetrahedra). When the mesh size increases, and as a consequence the average tetrahedron size decreases, the maximum allowed step size in each iteration of the MSM, has to be decreased to prevent unwanted "spring-flipping". This results in a more quadratic approximation for the MSM. It was noticed that a constant 40% time gain can be achieved with the MTM compared to FEM and MTM was on average 52% faster than MSM.

3. True validation

Before a soft tissue simulator can be used in routine clinical practice, it has to be shown that this simulator is able to give an accurate prediction of the new facial outlook after surgery. The only way to truly measure this accuracy is by comparing post-operative data with the predicted data (Schutyser et al., 2000; Chabanas et al., 2004; Zachow et al., 2004). This important validation step was often lacking in other work. In this section, we discuss how our validation data was acquired and processed. The validation work-flow includes following steps:

(1) *Data acquisition and pre-processing*. Patients undergo a pre- and post-operative CT scan. Out of the two CT data sets the skull and skin surface are reconstructed. A tetrahedral volumetric mesh that serves as input for the soft tissue simulation, is built after first segmenting the facial soft tissues out of the pre-operative CT data.

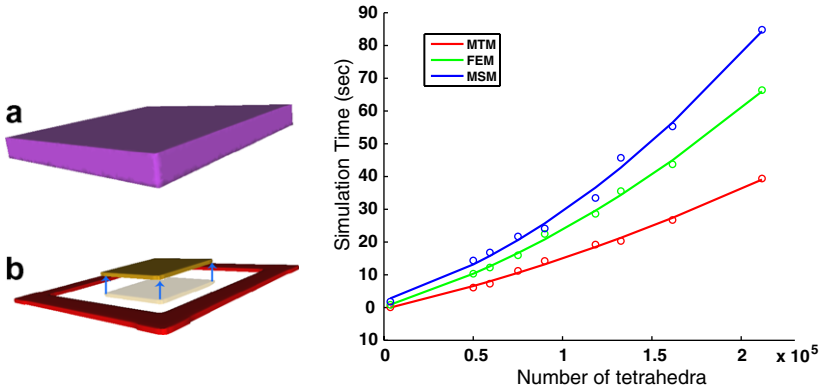

Fig. 2. Left: (a) virtual test cube and (b) boundary conditions applied to this cube. The centre of the cube (yellow) is moved 6 mm upwards, while the border (purple) is kept fixed. Right: Simulation time in function of the mesh size for all three biomechanical models. (For interpretation of the references to color in this figure legend, the reader is referred to the web version of this article.)

(2) *Bone-related planning*. A maxillofacial bone-related planning that corresponds to the real performed procedure is generated.
(3) *Generating boundary conditions*. Out of the bone-related planning boundary conditions for the biomechanical soft tissue model are generated.
(4) *Simulation*. The new facial outlook is computed using a specific computational strategy.
(5) *Validation*. The computed facial outlook is qualitatively and quantitatively compared with the real post-operative appearance.

While steps 1–3 are more straightforward, we introduce in step four a novel method to combine a very fast simulation with a high resolution of the visualisation result. In the next subsection we discuss our validation methods. All simulations were qualitatively and quantitatively validated. To quantitatively validate the predicted facial outlook, we measured distances between corresponding points of the predicted and post-operative facial outlook. Finally, in the last part of this section, we present the results of using this validation set-up on a database of 10 patients who underwent a maxillofacial procedure.

3.1. Data acquisition and pre-processing

When a patient needs to undergo a maxillofacial surgery, pre-operative a CT scan is acquired. Dense, highly detailed skin and bone surfaces are extracted with the marching cube algorithm with appropriately chosen thresholds (Lorensen and Cline, 1987).

To simulate the soft tissue deformations caused by a maxillofacial procedure, we also need a volumetric tetrahedral mesh containing all the facial tissues. Starting from the patient's CT data we automatically segment these facial soft tissues using a levelset segmentation algorithm (Ibanez et al., 2005). Out of this segmented data we can build with the Amira software (TGS, Merignac Cedex, France) a tetrahedral mesh. Since our levelset segmentation algorithm produces a very smooth segmentation, we never experienced any problem in obtaining an appropriate tetrahedral mesh. The design of a simulator that can be applied in routine clinical practice imposes constraints concerning processing time and memory usage, i.e. on the dimensions of these tetrahedral volumetric meshes. Therefore, it is interesting to restrict the tetrahedral mesh to the zone of the human face that will deform during surgery and to limit the number of tetrahedrons (typically less then 100,000).

In their clinical routine, all patients had a post-operative CT scan four months after surgery, when swelling has disappeared. These post-operative images are also used during our validation procedure. Therefore the post-operative CT data is first rigidly registered to the pre-operative CT data, using maximization of mutual information on an unaltered subvolume (Maes et al., 1997). From these co-registered post-operative data, a surface representation of the skin and skull are generated.

3.2. Bone-related planning

Maxilim (Medicim, Sint-Niklaas, Belgium) is a 3D bone-related planning system for maxillofacial surgery, originating from development in our group over the last years (Poukens et al., 2003). This software allows the maxillofacial surgeon to pre-operatively determine the necessary bone displacements and to see the effect of the procedure.

Since we want to validate the accuracy of our soft tissue simulator, we have to ensure that the planned procedure is exactly the same as the one performed by the surgeon. There are two critical parameters when planning a maxillofacial intervention: determination of the cut surfaces and determination of the displacements of the different skull parts. To define these parameters we use the pre-operative skull surface and the co-registered post-operative skull representation, generated as discussed in Section 3.1.

During surgery the skull was cut into a number of separate parts which where displaced independently and which can be easily identified on the co-registered post-operative skull surface by visual inspection. To transfer the location

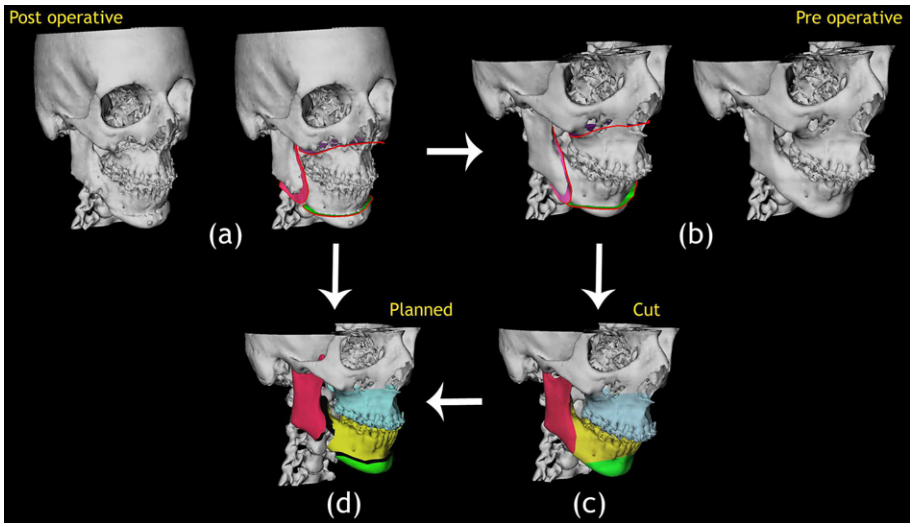

Fig. 3. Reconstruction of a bone-related planning that resembles the performed procedure as much as possible.

of the cut surfaces from the co-registered post-operative to the pre-operative skull representation, we first divide this post-operative skull surface in different patches that each correspond to a separate skull part (see Fig. 3a). Each post-operative surface patch is then separately matched by manual alignment to the pre-operative skull representation. Afterwards the ICP algorithm (Groeve et al., 2001) is used to refine the rigid registration (Fig. 3b). The outline of each registered patch on the pre-operative skull surface as defined by ICP, is then used to define an initial cut surface on the pre-operative skull (Fig. 3c). Then the pre-operative skull was virtually cut with these cut surfaces. Finally, the resulting bone fragments are again registered to the co-registered post-operative skull surface using ICP, to precisely determine the displacement of each skull part (Fig. 3d). The ICP algorithm was initialised by a manual allineation of the different skull parts.

This work-flow enables us to reconstruct the performed surgery accurately. However, some differences between the planned procedure and the co-registered post-operative skull which cannot be corrected by rigid displacements of bone parts, remained. The most important reasons for these mismatches are misplacement of a cut surface due to metal streak artifacts on the CT data, bone growth after surgery and placement of screws in the bone during surgery. As a consequence the maximal distance between the planned skull and the co-registered post-operative skull, remained around 1 mm.

3.3. Boundary conditions

To simulate the effect of a maxillofacial surgery on the soft tissues, the bone-related planning has to be mapped to the tetrahedral soft tissue model. Therefore, we assume that the motion of a soft tissue point that adjoins the skull, equals the motion of that part of the skull. In this way two types of points can be distinguished: join points and free points (see Fig. 4).

- *Join points*. All points that join at a part of the skull. This skull part will be kept fixed or will be repositioned during surgery.
- *Free points*. All the other soft tissue points are free. During simulation their movement is completely determined by the resulting elastic force that exists in these points.

In the present simulator, we do not model the exact contact behaviour between lips and teeth. At this moment teeth are treated as any other part of the skull, while a sliding contact behaviour would be more realistic and could probably improve simulation results.

3.4. Simulation

The created tetrahedral mesh and boundary conditions serve as an input for our soft tissue simulator. We used four different computational strategies (see Section 2) to model the facial soft tissue behaviour and to predict the patient's post-operative appearance. These four models are a linear FEM, a non-linear FEM, a MSM and a MTM. During simulation first join points are displaced as defined by the boundary conditions. Next, the new posi-

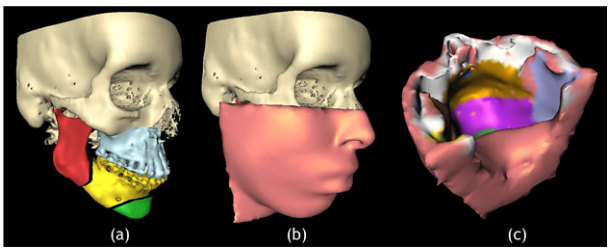

Fig. 4. Determination of the boundary conditions: (a) the bone-related planning; (b) the planning data is mapped to the soft tissue model; and (c) pink points are free points, the other colored points are join points. The movement of a join point equals the movement of the corresponding skull part. (For interpretation of the references to color in this figure legend, the reader is referred to the web version of this article.)

tion of each free model point is searched by demanding that the total elastic force should be zero in this point when the object is in rest. Since we assume the facial tissues to be homogeneous and isotropic, it can easily be shown that the equations that need to be solved, are independent of Young's Modulus for all four computational strategies. For the linear and non-linear FEM and the MTM the Poisson Ratio was set to 0.46 during all simulations (Fung, 1993).

As mentioned in Section 3.1, for reasons of computational efficiency the tetrahedral mesh used for simulation is restricted to only the zone of the human face that will deform during surgery and is quite smooth due to the limited number of tetrahedrons. The recognition value of such a smoothed mesh is however rather low, as shown in Fig. 5a. Moreover, since the perception of the human face is mainly determined by the relationship between different parts of the face, it is important for the surgeon to see the whole face and not just a part of it when inspecting the effect of a maxillofacial procedure. As a result, this tetrahedral mesh is unsuitable for clinical validation. To combine the advantages of a smooth sparse tetrahedral mesh for fast simulations and a very dense, highly detailed mesh for a good recognition, we introduce a volume/surface mapping method.

With the volume/surface mapping method, we first calculate the new facial outlook using a smooth sparse tetrahedral mesh and we then map this deformation field to a dense triangle representation of the human skin surface, that was also generated during pre-processing of the data (see Section 3.1). Since the tetrahedral mesh is much sparser than the skin surface, we have to interpolate the calculated deformation field.

We suggest two different interpolation strategies. First, the linear FEM shape functions (Zienkiewicz and Taylor, 2000) can be used to calculate the displacement in every point of the triangular surface. Second, an inverse distance weighted interpolation strategy is presented. Both methods enclose two steps: an initialisation procedure and an update process during which the displacement in each point of the triangular surface is calculated.

For the first method, the shape function method, we search during initialisation for each point P_i of the triangular skin surface the tetrahedron that is closest to this point P_i. To find this tetrahedron we project point P_i onto the outer triangular surface of the tetrahedral mesh and we define the tetrahedron that contains triangle k where point P_i was projected on, as the closest tetrahedron of this point. In the update stage the displacement of every surface point P_i is determined using the FEM shape functions of the closest tetrahedron:

$$u(P_i) = -\sum_{j=0}^{3} \frac{m_j(P_i - q^0_{j+1})}{6V_T} u_j \tag{13}$$

with $q^0_{j=0,\ldots,3}$ and $u_{j=0,\ldots,3}$ the initial position and displacement of the four vertices of this tetrahedron, V_T the initial tetrahedron volume and $m_{j=0,\ldots,3}$ are the area vectors for each vertex as defined in (Cotin et al., 2000).

The second approach uses a more simple inverse distance weighted interpolation strategy. We initialise the interpolation scheme by searching for each point Q_j of the outer surface of the tetrahedral mesh, the corresponding point P_i on the triangular skin surface. Since this skin surface is very dense, we can assume that the corresponding point P_i is simply the closest point on the triangular surface. To calculate the displacement of each surface point, we first map the displacement of each point Q_j of the tetrahedral mesh to its corresponding point of the facial skin surface. The displacement of n points of the facial skin surface is now known. Next, the displacement of every point P_i of the facial skin surface is found by using following interpolation scheme between these n points:

$$u(P_i) = \frac{\sum_{\forall j \in \Theta_i(x,y)} \frac{u(P_j)}{d_{ij}}}{\sum_{\forall j \in \Theta_i(x,y)} \frac{1}{d_{ij}}} \tag{14}$$

with $u(P_i)$ the displacement of point P_i, d_{ij} the distance between point P_i and P_j and $\Theta_i(x,y)$ the collection of all points that lie in sphere with a radius of x mm around point P_i and have a connectivity with this point P_i lower than y. Empirically, 3 and 5 mm were assigned to x and y, respectively.

In Fig. 5, we show the result of the volume/surface mapping visualisation method using both interpolation strategies. As can be seen, the high detail deformed skin surfaces (figure d and e) allow a much better and more realistic visual inspection of the effect of the maxillofacial surgery. In Section 3.6.1, both interpolation strategies will be quantitatively compared.

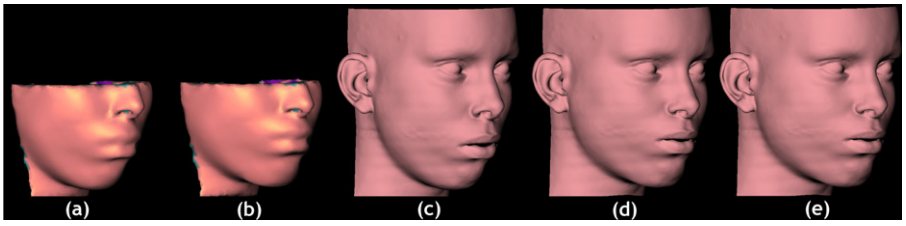

Fig. 5. (a) The initial tetrahedral mesh, (b) the deformed tetrahedral mesh, (c) the initial skin surface, (d) and (e) the deformed skin surfaces generated, respectively, with the shape function method and the inverse distance weighted interpolation approach.

3.5. Validation procedure

We validated the predicted new facial outlook in two ways: quantitatively and qualitatively. For the qualitative validation surgeons were asked to rate the prediction result by visual inspection. Quantitative validation implies measurement of the distances between corresponding points of the predicted and real post-operative facial skin surface.

3.5.1. Quantitative validation

Quantitative validation incorporates measuring distances between the predicted and post-operative facial skin surface. Typically, for these measurements, the predicted and post-operative facial skin surface are first rigidly registered based on an unaltered subvolume and subsequently the distance between both surfaces is determined. The distance measurement can be a two-sided Hausdorff distance (Zachow et al., 2004) or a signed Euclidean distance (Schutyser et al., 2000; Chabanas et al., 2004; Mollemans et al., 2004). Afterwards the generated distance map can be visualised or statistically analysed.

As highlighted by Chabanas et al. (2004) the main problem of these distance maps is an underestimation of the real error, since the map is calculated as the minimal Euclidean distance between points of the predicted and the real post-operative skin surface and not as the distance between corresponding points. To overcome this problem, a method was elaborated that is capable of finding a better estimate of the correspondences between both facial surfaces.

First we rigidly register the pre-operative and post-operative CT data using maximization of mutual information on an unaltered subvolume (Maes et al., 1997), typically the top of the skull, and extract out of these data sets the pre-operative and co-registered post-operative facial skin surface (see also Section 3.1). During simulation the predicted facial skin surface is calculated by deforming the pre-operative facial skin surface (Section 3.4). For finding 'true' correspondences between this predicted facial skin surface and the co-registered post-operative skin surface, we used a variant of the non-rigid TPS-RPM algorithm (Chui and Rangarajan, 2000; Chui and Rangarajan, 2003).

The original TPS-RPM algorithm finds correspondences between a moving and a target set of points A and B, by defining a regularized transformation $\mathbf{f}$: A $\rightarrow$ B. This regularisation ensures that the internal structure of point set A is taken into account during the registration process, which can be achieved by minimising following cost-function:

$$E_{\mathrm{TPS}} = \sum_{j=1}^{N} \|b_i - f(a_i)\|^2 + \lambda \int\int\int \left[\left(\frac{\partial^2 f}{\partial^2 x^2}\right)^2 + \left(\frac{\partial^2 f}{\partial y^2}\right)^2 + \left(\frac{\partial^2 f}{\partial z^2}\right)^2 + 2\left(\frac{\partial^2 f}{\partial x \partial y}\right)^2 + 2\left(\frac{\partial^2 f}{\partial x \partial z}\right)^2 + 2\left(\frac{\partial^2 f}{\partial \partial y \partial z}\right)^2 \right] \mathrm{d}x\,\mathrm{d}y\,\mathrm{d}z \tag{15}$$

with a_i and b_i corresponding points of sets A and B, respectively. The second term is a measure for the total curvature of the transformation which constrains the smoothness of the transformation. The influence of this constraint is controlled by a parameter λ. The transformation function $\mathbf{f}$ is defined as a thin-plate spline (TPS) function:

$$f(a_i) = a_i \mathbf{D} + \phi(a_i)\mathbf{W} \tag{16}$$

in which $\mathbf{D}$ is an affine transformation matrix, $\phi(x)$ the used spline kernel and $\mathbf{W}$ a non-affine transformation coefficient matrix.

At initialisation the correspondences between data set A and B are unknown. Hence, it is impossible to calculate the transformation $\mathbf{f}$ in one step. Therefore, the original TPS-RPM algorithm defines a correspondence matrix $\mathbf{M}$ which keeps track of the current estimated correspondences between data set A and B. If point set A and B contain K and N points, respectively, the new energy function that needs to be optimised is given as

$$E_{\mathrm{TPS}} = \sum_{j=1}^{N}\sum_{i=1}^{K} m_{ij}\|b_j - f(a_i)\|^2 - \zeta \sum_{j=1}^{N}\sum_{i=1}^{K} m_{ij} + \lambda \int\int\int \left[\left(\frac{\partial^2 f}{\partial^2 x^2}\right)^2 + \left(\frac{\partial^2 f}{\partial y^2}\right)^2 + \left(\frac{\partial^2 f}{\partial z^2}\right)^2 + 2\left(\frac{\partial^2 f}{\partial x \partial y}\right)^2 + 2\left(\frac{\partial^2 f}{\partial x \partial z}\right)^2 + 2\left(\frac{\partial^2 f}{\partial \partial y \partial z}\right)^2 \right] \mathrm{d}x\,\mathrm{d}y\,\mathrm{d}z \tag{17}$$

To minimise this energy function a deterministic annealing procedure is used. Starting at a high temperature value T for λ the algorithm will only allow the points to move in a group fashion way. As the temperature decreases this constraint loses its importance and this allows the points to move more locally to satisfy the minimum energy-condition.

Although this TPS-RPM algorithm has proven to be quite accurate in finding corresponding points, it is known to be quite resource-hungry and does not scale very well. As a consequence the original TPS-RPM algorithm can only be used for non-dense meshes. Usages of such non-dense meshes would induce a larger registration error, due to the discretization, that would strongly influence the final result of our quantitative validation. Therefore, Tondeur et al. (2006) implemented a variant of this TPS-RPM algorithm that uses the same TPS transformation but searches correspondences between a point set and a continuous surface description.

Consider two point sets: a moving set A and a target set B. To obtain a continuous representation of the target set a radial basis function (RBF) is fitted through this point set. Next following iterative scheme can be used, to obtain the transformation between both data sets:

Initialization

Load the moving set A (P_{A})
$P_{\mathrm{corr}} = P_{\mathrm{A}}$
Fit a RBF trough target set B ($\mathrm{RBF_B}$)
Temperature parameter $T = T_{\mathrm{init}}$

Outer Iteration : Deterministic annealing
  Inner Iteration : Register moving set at target set
    $P_{temp} = P_{corr} + \mu(P_{corr})\text{grad}(P_{corr})$
    (with grad the gradient of RBF_B and $\mu(x)$ the step size.
    This step size is proportional to RBF_B in point x)
    Use TPS (Eq. (17)) to calculate the transformation **f** from P_A to P_{temp}
    $P_{corr} = \mathbf{f}(P_A)$
  Until Convergence
  Decrease temperature T
Until final T is reached

All RBF and TPS calculations are performed using the FastRBF Toolbox (Farfield Technology, Christchurch, New Zealand), which implements specialised fast evaluation and generation techniques for RBF's and makes these RBF's applicable for large data sets.

The effect of the non-rigid warping, compared to a closest point search, can clearly be seen in Fig. 6. Left the predicted facial skin surface is shown. On this surface well defined facial points were manually indicated. Next the corresponding points on the real post-operative facial surface were searched using a traditional closest point approach (green points) and the introduced non-rigid algorithm (purple points). When zooming in on the lip area, a clear difference between both approaches is noticed. Thanks to the regularized warping of the algorithm, a better estimate of the 'true' correspondences between the predicted and real post-operative skin surface is achieved, resulting in a more correct distance measurement.

For our validation study we search correspondences between all mesh points of the predicted triangular skin surface, typically around 60,000 points, and the co-registered post-operative skin surface. Afterwards a signed euclidean distance between these corresponding points is measured. The measured distances are visualised by projecting these distances onto the facial skin surface by means of a color-code. This results in an easy interpretable image of the error distribution over the facial skin surface. Second, we calculate following statistical properties for each distance map: the mean, the variance, the 50%, 90% and 95% percentiles of the distance distributions.

3.5.2. Qualitative validation

A validation procedure during which surgeons are asked to score the predicted facial outlook, was set up to measure the value of the soft tissue simulations qualitatively. Predictions of the new facial outlook were calculated using the MTM. The qualitative validation procedure includes two experiments:

- *Experiment 1*. First for each patient the pre-operative facial skin surface, pre-operative skull and planned skull surface are shown to the surgeon. The surgeon can inspect these models in a 3D environment (see Fig. 7). Texture, obtained with a 3D camera system (Eyetronics, Leuven, Belgium) was added to the facial skin surface to increase realism. Based on the inspection of these models and the planning data, the surgeon is asked to imagine the patient's post-operative facial appearance. When ready, we show him our predicted new facial outlook and ask him to score on a scale of 1–5 the truthfulness of this prediction. In the 3D environment, it is possible to switch fast between the pre-operative and predicted facial skin surface to emphasise the deformation between both surfaces. Finally, the surgeon is asked to indicate on the face the regions where he thinks big errors between the predicted facial skin surface and real post-operative skin surface are present.
- *Experiment 2*. In the second experiment, the surgeon is shown the pre-operative skin and skull surface, the predicted new facial outlook and the planned skull, like in the first experiment. However, in this experiment also a second 3D viewer is given in which the real post-operative facial surface can be inspected (Fig. 8). Based on these shown data the surgeon has to score two statements on a 1–5 scale. First he has to validate the resemblance between the predicted facial outlook and real post-operative appearance. In a second stage we ask him to once again score the truthfulness of the predicted facial skin surface, after having now seen the real post-

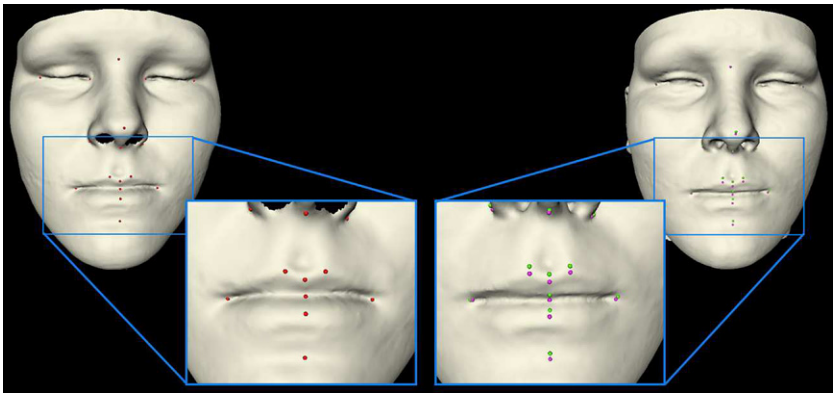

Fig. 6. Well-defined facial points were indicated on the predicted facial outlook (left). The corresponding points on the post-operative facial appearance (right) are searched with a traditional closest point algorithm (green points) and a variant of the non-rigid TPS-RPM algorithm (purple points). (For interpretation of the references to color in this figure legend, the reader is referred to the web version of this article.)

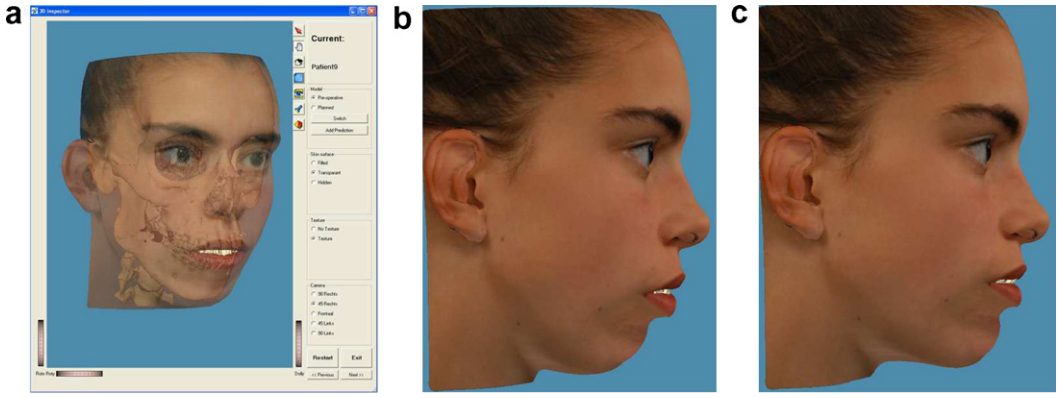

Fig. 7. Qualitative validation procedure: (a) surgeons could inspect the pre-operative facial skin surface, pre-operative skull and planned skull surface in a 3D environment. Next they are asked to score the truthfulness of the predicted post-operative skin surface; (b) shows the textured pre-operative facial skin surface of a patient; and (c) the predicted post-operative facial appearance.

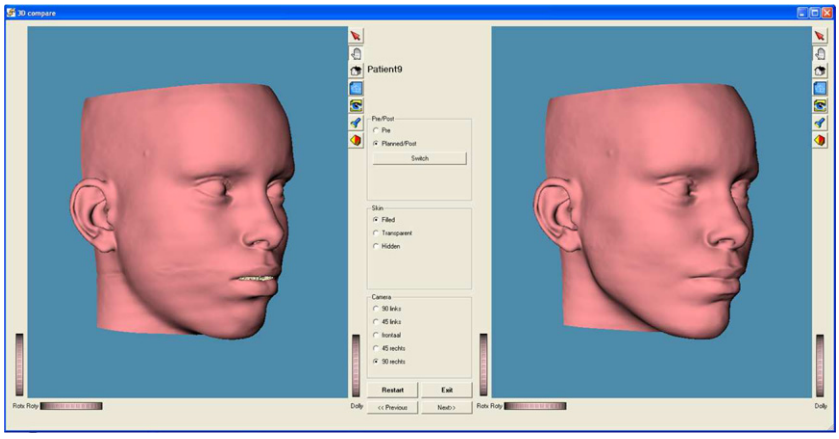

Fig. 8. The second qualitative validation experiment. Left the predicted facial skin surface is shown, right the real post-operative appearance is visualised.

operative facial appearance. At last he has to define the facial regions where the predicted and real post-operative skin surface differ the most, in his opinion.

With the first experiment we want to measure how correct and realistic our predictions are, not knowing the real post-operative appearance. In the second test we want to define what are most error-sensitive facial regions, e.g. maybe it does not matter if large errors arise in the cheek area, but is it important to accurately predict the chin contour. Furthermore we want to investigate if a facial skin surface that was scored as truthful in the first experiment, still gets a high score after seeing the real post-operative facial skin surface in the second experiment.

Besides these two experiments we asked the surgeon to answer some more general questions concerning the relevance and practicability of 3D soft tissue predictions for maxillofacial surgery.

3.6. Results

In close cooperation with Dr. Nadjmi (Eeuwfeestkliniek, Antwerpen, Belgium), we acquired data sets of 10 patients who underwent a maxillofacial procedure. For all patients we used the work-flow as described above, to process the data. The patient group counts 2 Class III and 8 Class II patients (Sarver, 1997).

The eight columns of Table 2 summarize the data set number, the surgical procedure for each patient, the number of tetrahedrons used in each model, the maximal movement of the soft tissue points during simulation and the time needed to calculate the new facial outlook for each patient using one of the four computational strategies. All calculations were performed on a standard personal computer with an Intel Pentium 4 processor and 1 Gbyte RAM. As expected the non-linear FEM is a lot slower as the three other linear computational strategies. Unexpectedly, FEM turns out to be faster than MSM. The MTM clearly beats FEM and MSM in simulation time. As shown in the last row of Table 2 the average simulation time of the MTM equals more or less 10 s. These very short simulation times are a great advantage for an interactive maxillofacial surgery planning system.

3.6.1. Quantitative results

For the quantitative validation step the 10 data sets were processed as discussed in 3.5.1. To improve the validation the eye region and neck area of each patient were manually

Table 2
A database of 10 patients was acquired

Data set	Procedure	N_{tetra}	M_{max} (mm)	T_{FEM} (s)	T_{MTM} (s)	T_{MSM} (s)	T_{NFEM} (s)
P1	MSB + G	129,955	8.1	24.7	16.5	68.35	893.6
P2	G + MxA	74,232	9.5	11.9	7.6	24.3	233.4
P3	MSB + MxA	85,213	4.9	16.8	6.6	22.7	449.1
P4	MA	66,286	4.3	13.7	2.5	10.99	41.1
P5	MA + G + MxA	79,716	16.7	19.2	12.9	47.6	1885.2
P6	MA + MxA	79,125	6.3	19.5	5.4	33.1	913.5
P7	MA + MxA	75,314	9.6	17.9	9.9	32.2	1001.6
P8	MA + G + MxA	30,3745	9.9	104.1	23.2	94.3	2712.3
P9	MA + G + MxSB	80,654	13.8	11.5	8.2	42.3	897.3
P10	MA + G + MxA	91,925	9.5	17.9	8.5	34.6	498.6
Mean		106,616	9.26	25.7	10.2	35.1	952.6

Code	Description
MSB	Mandibular Set Back
MA	Mandibular Advancement
G	chin Genioplasty
MxSB	Maxillary Set Back
MxA	Maxillary Advancement

For each patient a soft tissue model was built and the new facial outlook was calculated based on the performed surgery and using one of the 4 computational strategies: FEM, MTM, MSM and NFEM. The first two columns show the performed maxillofacial procedure and the number of tetrahedra used in the facial soft tissue model. Column three lists the maximum movement over all soft tissue points during simulation. Time needed to calculate the new facial outlook is summarized for each strategy in the last four columns.

selected and omitted during processing. Differences in these regions are mainly due to opening or closing of the eyelids or a change in head position during acquisition of the pre-operative and post-operative CT scan and cannot be simulated by our soft tissue prediction system. Fig. 9 summarizes the outcome of the statistical analysis for all four computational models. In the first row we show the mean, the variance and the maximum of the distance maps for each patient. The second row presents the 50%, 90%, 95% percentiles of the distance distributions of the generated maps. In Table 3 we summarize more numerical data of the outcome of the statistical analysis, showing average values over all data sets for the 50%, 90% and 95% percentiles of the distance distributions of the generated maps for FEM, MTM, MSM and NFEM.

These results show that most accurate results are obtained with FEM and MTM and that both models calculate almost the same prediction result. Visual inspection

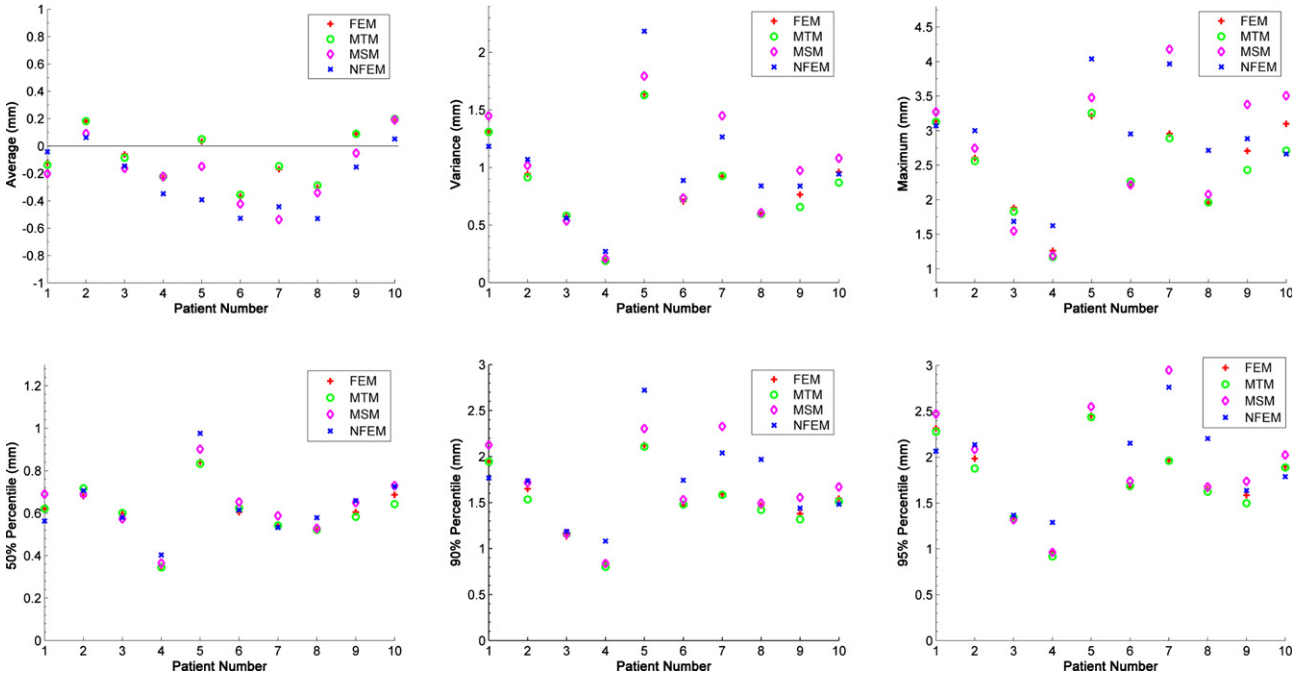

Fig. 9. For 10 patients, quantitative validation results of the predictions calculated using FEM, MTM, MSM or non-linear FEM, are presented.

Table 3
Average values, over all 10 patients, of the 50%, 90% and 95% percentiles of the distance maps calculated between the predicted and actual post-operative facial skin surface

Model	$T_{50\%}$	$T_{90\%}$	$T_{95\%}$
FEM	0.60	1.51	1.78
MTM	0.60	1.48	1.75
MSM	0.64	1.67	1.95
NFEM	0.63	1.71	2.05

of the predicted skin surfaces, showed that differences between both models are only located near the neck area, which is of less importance for the prediction quality. Also the prediction results obtained with the MSM are quite good. However, when deformations become large (P2, P7, P9 and P10) the MSM is clearly less accurate than FEM or MTM. Introduction of the non-linear FEM did not improve the simulation results. Only for P1 a better prediction was obtained when using the NFEM strategy. For all other data sets, the accuracy of the NFEM predictions was lower than those obtained with the three other computational strategies. As can be seen in Table 3 the mean $T_{50\%}$ for FEM and MTM is only 0.6 mm and the average $T_{90\%}$ equals 1.50 mm. Keeping in mind the stability and predictability of a maxillofacial surgery (around 1 mm), these distance values show an acceptable accuracy.

Besides the statistical analysis of the generated distance maps we can also project these distance maps on the model by means of a color-code. This is shown for predictions calculated with the MTM, in Fig. 10. This figure shows the projected distance maps for each of the 10 patients. The color map ranges between −3 mm and 3 mm, where a negative error means that the predicted skin surface lies behind the post-operative skin surface. When inspecting these images, it can be noticed that there are some typical regions with large errors, namely, the tip of the chin, the lips and the two area's besides the nose wings.

To investigate the difference between the inverse distance weighted and the shape function interpolation scheme, as introduced in Section 3.4, we measured the accuracy of the prediction results calculated with the MTM in combination with one of both mapping strategies. These results are summarized in Fig. 11 showing the 50%, 90% and 95% percentiles of the calculated distance maps. Average differences between both methods were smaller

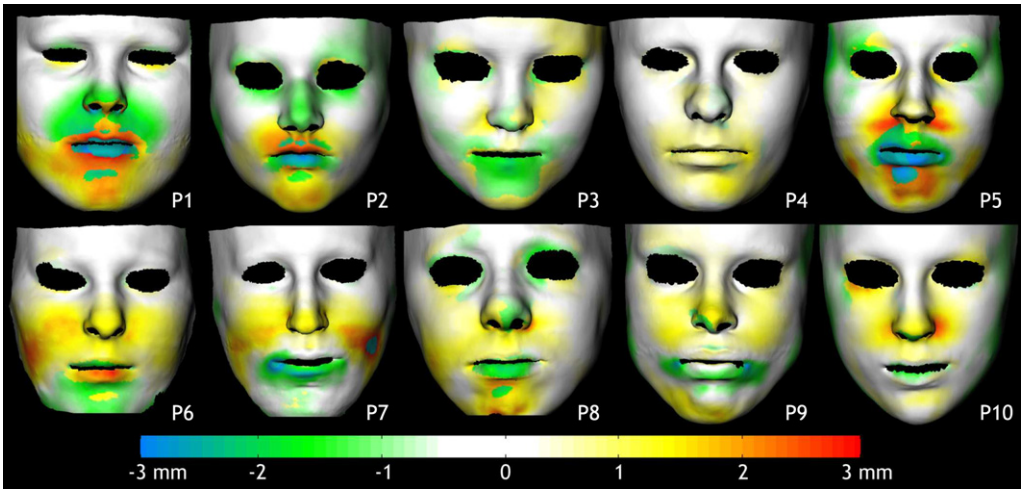

Fig. 10. Distance map visualised by color coding for the 10 patients. A negative error means that the predicted skin surface lies behind the post-operative skin surface.

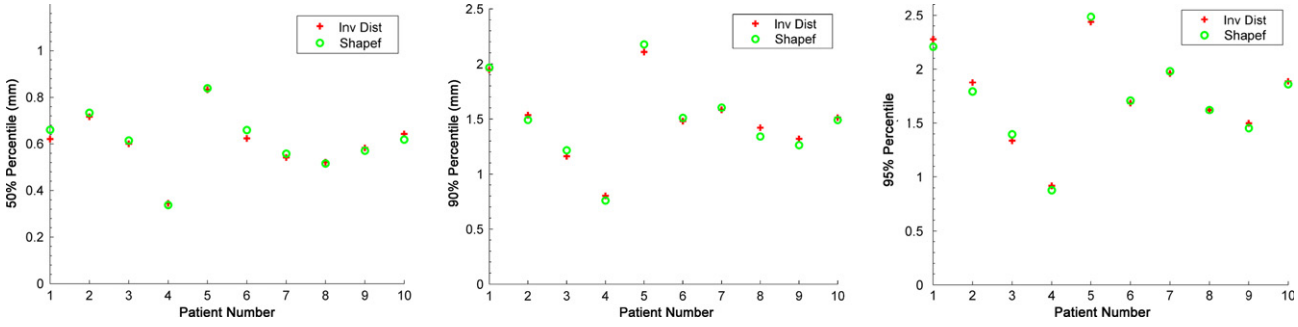

Fig. 11. The inverse distance weighted and shape function interpolation scheme were used to map the deformations calculated on the 3D tetrahedral mesh to the dense triangular skin surface. For both methods differences between the predicted and actual post-operative skin surface were measured.

Table 4
Calculation time results for the inverse distance weighted and shape function interpolation scheme

Data set	Inverse distance weighted		Shape function	
	A (ms)	B (ms)	A (ms)	B (ms)
P1	187	547	3813	1141
P2	63	109	859	219
P3	78	157	1188	344
P4	125	281	2203	688
P5	141	297	2094	625
P6	109	281	2172	594
P7	172	500	3532	1000
P8	140	312	3016	625
P9	156	454	3156	1047
P10	94	109	1094	250

Step A is the initialisation step, while in step B the actual interpolation is calculated.

than 0.05 mm for all three statistics. This difference is irrelevant for our application.

The time needed to calculate the interpolation can be separated in an initialisation step (step A) and an interpolation step (step B), as discussed in 3.4. These timing results are summarized for each patient in Table 4. The inverse distance weighted method clearly outperforms the shape function method in timing results with an average time gain of 85%. Considering the simulation times, listed in Table 2, we can conclude that there is a significant difference in calculation time between both methods.

3.6.2. Qualitative results

Our qualitative validation study, as described above, was carried out by eight maxillofacial surgeons. Experiment 1 was always filled in first, next the surgeon carried out experiment 2 and finished with the more general questionnaire. During each experiment, the data of all 10 patients was presented to the surgeon in a randomised order.

Table 5 summarizes the most frequent scores given by all surgeons for each of the 10 patients for the most relevant statements of experiments 1 and 2. A statement, with which the surgeon completely agreed, was rated with 5, while a 1 indicates total disagreement with the statement. The scores of the more general questions are depicted in Table 6.

It is noticed that the most frequent scores over all patients for statement S2 are not lower than 3 and the overall median score for this statement is 3.75, which implies that the shown prediction corresponds well to what the surgeon expected to be the actual post-operative facial appearance. The most frequent score for statement S3 are even a little bit higher (overall median score is 4), indicating that our predictions are rated as good or even slightly better, after seeing the real post-operative outlook. The answers to the more general questionnaire (Table 6), confirm these results. The interviewed surgeons agreed that this soft tissue prediction system could really help to make a better bone-related planning and to ameliorate communication between surgeon and patient.

4. Discussion

4.1. Computational strategies for soft tissue modelling

In this work we compared the usage of four different computational strategies for a 3D soft tissue maxillofacial planning system. These strategies are a linear Finite Element Model (FEM), a non-linear Finite Element Model (NFEM), a linear Mass Spring Model (MSM) and a linear Mass Tensor Model (MTM). This last model, based on the work of Cotin et al. (2000), is some sort of golden mean between MSM and FEM.

MSM and FEM, are frequently used to predict the new facial outlook after maxillofacial surgery. MSM has an easy architecture and low memory cost, but is not very biomechanical relevant and lacks sufficient accuracy for our clinical application. FEM does not have this drawback but has on the other hand a more complex architecture. Moreover, the speed of FEM is highly related to the sparsity of the global stiffness matrix, which may result sometimes in rather long simulation times. Although some

Table 5
Surgeons scored statements on a 1–5 scale

Statement	P1	P2	P3	P4	P5	P6	P7	P8	P9	P10
The performed bone-related surgery is clearly visualised (S1)	5	4	4.5	5	5	4.5	4	4	4.5	5
The prediction of the new facial outlook after surgery is correct (S2)	3.5	3	3	4	4	4	3	4	3	4
The predicted outlook is a good prediction of the actual post-op outlook (S3)	5	3	3	5	4	4.5	4	4	3.5	4

Statement S1 and S2 was scored during experiment 1. The last statement belongs to experiment 2.

Table 6
General questions concerning our 3D soft tissue prediction system, were rated by surgeons

Statement	Score
Prediction of the soft tissue deformations can improve the bone-related planning (S4)	5
This 3D soft tissue prediction system is useful in daily clinical practice (S5)	4
This prediction system can greatly improve communication between surgeon and patient (S6)	4.5

authors state that reducing the simulation time cannot be a goal of a maxillofacial soft tissue prediction system, we argue that soft tissue predictions should be incorporated during bone-related planning, as confirmed in the literature and by results of our qualitative validation study.

We introduced two novel extensions to the original MTM, a direct computation step and a local dynamic stop criterion, resulting in a very fast and accurate biomechanical model. As shown the usage of a stop criterion does not introduce new significant errors, since the MTM prediction can only have a limited accuracy. Moreover, an average time gain of more than 40% could be achieved compared to FEM or MSM.

The presented MTM, MSM and FEM are homogenous biomechanical models, which do not incorporate tissue specific behaviour. Westermark et al. (2005) investigated the effect of an inhomogeneous tissue model. He differentiated between fat and muscle tissue and assigned for each tissue type different values to the Modulus of Young (E) and the Poisson Coefficient (v). He concluded that the net improvement of using such inhomogeneous tissue models, did not significantly influence the prediction quality. Since his validation included only a single relevant data set, we hope to be able to affirm his results in the very near future by performing the same study on our more extensive database of 10 patients.

4.2. True validation

In the second part of this work, we presented results of a validation study for all four computational strategies on a data set of 10 patients, including pre-operative and post-operative image data. This validation study consists of two parts: a quantitative and qualitative validation.

For the quantitative validation we measured distances between corresponding points of the predicted and actual post-operative facial skin surface. Correspondences were searched using a variant of the non-rigid TPS-RPM algorithm. Measuring the minimal euclidean distance between both surfaces, would result in an underestimation of the prediction error, as highlighted in (Chabanas et al., 2004).

Highest accuracy was obtained by usage of the FEM or MTM approach. For the MTM we showed that the median prediction error over all 10 patients was below 0.6 mm and even the 90% percentile was smaller than 1.5 mm. The MSM results were comparable to the MTM results when the displacements were relatively small. However, for data sets with large displacements (P2, P5, P7 and P9) the accuracy of the MSM clearly decreased. Finally, introduction of an non-linear model, NFEM, did not improve the simulation accuracy. Only for data set P1 a slight increase in accuracy was recorded. The reduced accuracy for all other data sets, can perhaps be explained by the fact that this non-linear modelling is much more sensitive to several criteria like the mesh (which should be refined in high stress areas), the boundary conditions and elastic parameters of the model. This same conclusion was already made by Chabanas et al. (2004) based on some first results. Probably definition of more realistic boundary conditions, like the sliding contact behaviour between teeth and lips, is most necessary to further improve the simulation accuracy.

The quantitative validation study revealed that there are some typical regions with large errors: namely the tip of the chin, the lips and the two areas besides the nose wings. We think that the errors in chin and nose region are mostly due to the placement of screws on the bone during surgery; the extra displacement due to these screws, is not incorporated in our bone-related planning. Moreover, derivation of correct boundary conditions for the nose region is a very difficult task, since the nose bone is very thin and cannot be easily segmented. Finally, when looking to the lips, we suggest two main reasons why the lip movement is wrongly simulated. A first reason is the connection between lower and upper lip: in our soft tissue model the two lips are not explicitly separated from each other during simulation. Secondly, it was already noticed in the clinical relevant literature that the lower lip becomes more straight when the mandible is advanced during surgery and becomes more relaxed when the opposite is performed, our present model is clearly not able to predict this effect correctly.

Finally, during the quantitative validation study we compared prediction results obtained with two different interpolation strategies for the volume/surface mapping method. This volume/surface mapping enables the combination of short simulation times with a highly detailed visualisation of the deformed facial outlook. Results showed that using an inverse distance weighted interpolation scheme is significantly faster without loss of prediction accuracy compared to the usage of a more theoretical based shape function interpolation. The inverse distance weighted interpolation method has however as a drawback that it has to be tuned in function of typical mesh size of both the tetrahedral mesh and the triangular facial skin surface (see Section 3.4).

Besides a quantitative validation, also a qualitative validation of the predicted facial outlook, calculated with the MTM, for all 10 patients was performed. This qualitative validation included two well defined experiments. The study was carried out by eight surgeons and we can conclude that our predictions were rated as ‘good’ and ‘clinically relevant’ for all 10 patients.

It is interesting to compare results of this qualitative validation study, with results obtained during the quantitative validation study. First we note that the patient with the highest scores (P4) is also the patient with the lowest distance values in the quantitative validation approach. On the contrary, patients with the lowest scores (P2, P3 and P9) do not have the highest distance measurements in the quantitative analysis. Clearly a quantitative validation alone is not sufficient to separate good from bad predictions.

During experiments 1 and 2 of the qualitative validation, surgeons were asked to indicate regions of ‘high errors’ onto the predicted facial outlook. By comparing

these data with distance measurements of the quantitative validation we can define error-(in)sensitive facial regions. First, although patient P1, P6 and P7 have rather large errors in the cheek area these regions were never indicated as 'wrong' during the qualitative validation study by the surgeons. Secondly, it turned out that surgeons are very sensitive to errors in nose and lip region. For patient P1, P2 and P10 almost every surgeon indicated on the predicted facial skin surface the nose region as being wrongly simulated. Also when there was an inaccurate prediction of more than 1.5 mm of the lip contour, this was correctly noticed by the surgeons. At last for patient P2, P5, P8 and P9 there is a clear incorrect prediction of the post-operative chin outlook. It was noted that this inaccuracy probably arises from the fact that the patient's chin was in an unnatural tensed position during pre-operative CT acquisition, since patients were explicitly asked to close their mouth during this acquisition. Most surgeons stated that the soft tissue predictions would be strongly improved for these patients, if the chin had been more relaxed during CT acquisition.

Recently, Zachow et al. (2004, 2005) reported on a quantitative evaluation of 3D soft tissue predictions for maxillofacial surgery, based on a single data set. While their validation set-up is similar to ours and the simulation errors reported in (Westermark et al., 2005) are comparable to ours, our validation is more extensive as it includes 10 patients, showing consistent accuracy of all 10 cases. Moreover, our error measure is a more realistic and clinically more relevant measure than the full head averaged measures used in (Westermark et al., 2005), since we measure distances between corresponding points and only include the region of interest of the face, i.e. the deformed part of the face, and explicitly exclude the non-deformed parts such as the top of the skull.

Although most authors asked collaborating surgeons for feedback about their soft tissue simulations, none have presented an extensive qualitative validation. Since visualisation of the simulated facial appearance is the final goal of a maxillofacial soft tissue prediction system, we argue that a detailed qualitative validation study is essential. This validation should include well-defined experiments, during which statements have to be scored by the surgeon. As shown, results of such a qualitative validation and quantitative validation are not necessarily coherent. This incoherence enables the definition of new relevant research goals.

5. Conclusion

Maxillofacial surgery treats abnormalities of the skeleton of the head. Since the human face plays a key role in interpersonal relationships, people are very sensitive to changes to their outlook. Therefore, planning of the operation and reliable prediction of the facial changes are very important. Recently, the use of 3D image-based surgery planning systems is more and more accepted in this field. Although the bone-related planning concepts and methods are maturing, prediction of soft tissue deformation needs further fundamental research.

In this work, we compared four computational strategies to simulate the post-operative facial appearance: a linear Finite Element Model, a non-linear Finite Element Model, a Mass Spring Model and a new Mass Tensor Model. We introduced this last model and observed a significant time gain in simulation time compared to the two traditional used models: the linear Finite Element Model and the Mass Spring Model.

Before a soft tissue simulator can be used in clinical practice, the accuracy of the prediction of the new facial outlook after surgery needs to be assessed. We presented a work-flow for a quantitative and qualitative validation procedure, based on pre-operative and post-operative image data. A database of 10 patients was acquired and the qualitative validation was carried out by eight maxillofacial surgeons. For the quantitative validation distances between corresponding points of the predicted and actual post-operative facial outlook were measured for simulated data obtained with all four computational strategies. Best results were obtained by usage of the linear Finite Element Model or the Mass Tensor Model. We showed that for these model, the average median distance measures only 0.60 mm and the average 90% percentile stays below 1.5 mm. These results were confirmed by the qualitative validation study in which surgeons rated our predictions as 'good' and 'relevant' for usage in daily clinical practice.

In the near future, we hope to improve our soft tissue simulations even more. First the usage of an inhomogeneous biomechanical model, which distinguishes in mechanical behaviour of fatty and muscle tissue, will be further investigated. Next special attention will go to the nose and lip region, since these regions were defined as being most error-sensitive during our validation study. Defining proper boundary conditions for those regions and separating the under and upper lip in our volumetric soft tissue model, will be our primary future goals. Finally, we can conclude from this study that it is important that the patient's face is in a natural and relaxed position during CT acquisition. The definition of a clear clinical acquisition protocol is essential for further studies.

Acknowledgements

The authors thank Dr. R. Steffens, Dr. M. Martini, Dr. T. Appel, Dr. M. Wenghoefer and Dr. T. Erdsach (Klinik für Mund-, Kiefer- und Gesichtschirurgie Universitätsklinikum, Bonn, Germany), Dr. W.A. Borstlap (UMC St Radboud, Nijmegen, Netherlands) and Dr. B. Vanassche and Dr. N. Nadjmi (Eeuwfeestkliniek, Antwerpen, Belgium). They must be thanked for their voluntary participation in the qualitative clinical validation of this work. This work is part of the Flemish government IWT GBOU 020195 project on Realistic image-based facial modelling for forensic reconstruction and surgery simulation and K.U.Leuven/OF/GOA/2004/05.

References

Ackermann, M.J., 1998. The visible human project. Proceedings of the IEEE 86 (3), 504–511 (Special Issue on Virtual and Augmented Reality in Medicine).

Bianchi, G., Solenthaler, B., Szekely, G., Harders, M., 2004. Simultaneous topology and stiffness identification for mass-spring models based on fem reference deformations. Lecture Notes in Computer Science (MICCAI) 3217, 293–301.

Bro-Nielsen, M., Cotin, S., 1996. Real-time volumetric deformable models for surgery simulation using a finite elements and condensation. Computer Graphics Forum (Eurographics '96) 15 (3), 57–66.

Burk, D.L., Mears, D.C., Cooperstein, L.A., Herman, G.T., Udupa, J.K., 1986. Three-dimensional computed tomographic imaging and interactive surgical planning. The Journal of Computed Tomography 10 (1), 1–10.

Chabanas, M., Luboz, V., Payan, Y., 2003. Patient specific finite element model of the face soft tissues for computer-assisted maxillofacial surgery. Medical Image Analysis 7 (2), 131–151.

Chabanas, M., Marécaux, C., Chouly, F., Boutault, F., Payan, Y., 2004. Evaluating soft tissue simulation in maxillofacial surgery using preoperative and postoperative CT scans. In: Proceedings of CARS, pp. 419–424.

Chabanas, M., Payan, Y., Marécaux, C., Swider, P., Boutault, F., 2004. Comparison of linear and non-linear soft tissue models with post-operative ct scan in maxillofacial surgery. Lecture Notes in Computer Science (ISMS) 3078, 19–27.

Chui, H., Rangarajan, A., 2000. A feature registration framework using mixture models. In: Proceedings of the IEEE Workshop on Mathematical Methods in Biomedical Image Analysis (MMBIA), pp. 190–197.

Chui, H., Rangarajan, A., 2003. A new point matching algorithm for non-rigid registration. Computer Vision and Image Understanding 89 (2-3), 114–141.

Cotin, S., Delingette, H., Ayache, N., 1999. Real-time elastic deformations of soft tissues for surgery simulations. IEEE Transactions on Visualization and Computer Graphics 5 (1), 62–73.

Cotin, S., Delingette, H., Ayache, N., 2000. A hybrid elastic model allowing real-time cutting, deformations and force-feedback for surgery training and simulation. The Visual Computer 16 (8), 437–452.

Cousley, R.R., Grant, E., Kindelan, J.D., 2003. The validity of computerized orthognathic predictions. Journal of Orthodontics 30 (2), 149–154.

Dhondt, G., 2004. The Finite Element Method for Three-dimensional Thermomechanical Applications. Wiley.

Everett, P., Seldin, E.B., Troulis, M., Kaban, L.B., Kikinis, R., 2000. A 3D system for planning and simulating minimally-invasive distraction osteogenesis of the facial skeleton. Lecture Notes In Computer Science (MICCAI) 1935, 1029–1039.

Farkas, L.G., 1994. Anthropometry of the Head and Face, second ed. Lippincott Williams and Wilkins.

Fung, Y.C., 1993. Biomechanics: Mechanical Properties of Living Tissues. Springer, pp. 242–320 (Chapter 7).

Gelder, A.V., 1998. Approximate simulation of elastic membranes by triangulated spring meshes. Journal of Graphics Tools 3 (2), 21–42.

Gladilin, E., 2002. Biomechanical Modeling of Soft Tissue and Facial Expressions for Craniofacial Surgery Planning. Ph.D. Thesis, Fachbereich Mathematik und Informatik der Freien Universität Berlin, Konrad-Zuse-Zentrum für Informationstechnik Berlin (ZIB), October 2002.

De Groeve, P., Schutyser, F., Van Cleynenbreugel, J., Suetens, P., 2001. Registration of 3D photographs with spiral CT images for soft tissue simulation in maxillofacial surgery. Lecture Notes in Computer Science (MICCAI) 2208, 991–996.

Hofer, M., Strauß, G., Koulechov, K., Dietz, A., 2005. Definition of accuracy and precision - evaluating CAS-systems. In: Proceedings of CARS, pp. 548–552.

Ibanez, L., Schroeder, W., Ng, L., Cates, J., 2005. The ITK Software Guide. Kitware Inc.

Keeve, E., Girod, S., Kikinis, R., Girod, B., 1998. Deformable modelling of facial tissue for craniofacial surgery simulation. Computed Aided Surgery 3 (5), 228–238.

Kershaw, D.S., 1978. The incomplete cholesky-conjugate gradient method for the iterative solution of systems of linear equations. Journal of Computational Physics 26, 43–65.

Koch, R.M., Gross, M.H., Carls, F.R., von Büren, D.F., Frankhauser, G., Parish, Y.I.H., 1996. Simulating facial surgery using finite element models. Proceedings of SIGGRAPH. ACM Press, pp. 421–428.

Lee, Y., Terzopoulos, D., Walters, K., 1995. Realistic modeling for facial animation. Computer Graphics (Annual Conference Series) 29, 55–62.

Lorensen, W.E., Cline, H.E., 1987. Marching cubes: a high resolution 3D surface construction algorithm. In: Proceeding of SIGGRAPH, pp. 163–169.

Maes, F., Collignon, A., Vandermeulen, D., Marchal, G., Suetens, P., 1997. Multimodality image registration by maximization of mutual information. IEEE Transactions on Medical Imaging 16 (2), 187–198.

Meehan, M., Teschner, M., Girod, S., 2003. Three-dimensional simulation and prediction of craniofacial surgery. Orthodontics and Craniofacial Research 6 (Suppl. 1), 102–107.

Mollemans, W., Schutyser, F., Van Cleynenbreugel, J., Suetens, P., 2003. Tetrahedral mass spring model for fast soft tissue deformation. Lecture Notes in Computer Science (IS4TM) 2673, 145–154.

Mollemans, W., Schutyser, F., Van Cleynenbreugel, J., Suetens, P., 2004. Fast soft tissue deformation with tetrahedral mass spring model for maxillofacial surgery planning systems. Lecture Notes in Computer Science (MICCAI) 3217, 371–379.

Mollemans, W., Schutyser, F., Nadjmi, N., Suetens, P., 2005. Very fast soft tissue predictions with mass tensor model for maxillofacial surgery planning systems. In: Proceedings of CARS, pp. 491–496.

Picinbono, G., Delingette, H., Ayache, N., 2003. Non-linear anisotropic elasticity for real-time surgery simulation. Graphical Models 65 (5), 305–321.

Poukens, J., Schutyser, F., Van Cleynenbreugel, J., Riediger, D., 2003. 3D planning of distraction osteogenesis with maxilim software. In: Proceedings of the Fourth International Congress of Maxillofacial and Craniofacial Distraction, pp. 251–254.

Roose, L., De Maerteleire, W., Mollemans, W., Suetens, P., 2005. Validation of different soft tissue simulation methods for breast augmentation. In: Proceedings of CARS, pp. 485–490.

Saad, Y., Schultz, M.H., 1986. GMRES: a generalized minimal residual algorithm for solving nonsymmetric linear systems. SIAM Journal on Scientific and Statistical Computing archive 7 (3), 856–869.

Sarti, A., Gori, R., Lamberti, C., 1999. A physically based model to simulate maxillo-facial surgery from 3D CT images. Future Generation Computer Systems 15 (2), 217–221.

Sarver, D., 1997. Esthetic Orthodontics and Orthognathic Surgery, first ed. Mosby.

Schutyser, F., Van Cleynenbreugel, J., Ferrant, M., Schoenaers, J., Suetens, P., 2000. Image-based 3D planning of maxillofacial distraction procedures including soft tissue implications. Lecture Notes in Computer Science (MICCAI) 1935, 999–1007.

Schwartz, J.-M., Deniger, M., Rancourt, D., Moisan, C., Laurendeau, D., 2005. Modeling liver tissue properties using a non-linear visco-elastic model for surgery simulation. Medical Image Analysis 9 (2), 103–112.

Smith, J.D., Thomas, P.M., Proffit, W.R., 2004. A comparison of current prediction imaging programs. American Journal of Orthodontics and Dentofacial Orthopedics 125 (5), 527–536.

Terzopoulos, D., Walters, K., 1990. Physically-based facial modelling, analysis and animation. Visualization and Computer Animation 1 (4), 73–80.

Teschner, M., 2001. Direct Computation of Soft-tissue Deformation in Craniofacial Surgery Simulation. Ph.D. Thesis, Shaker Verlag, Aachen, Germany (January 2001).

Tondeur, S., Claes, P., Vandermeulen, D., Suetens, P., 2006. Regularized On-rigid ICP Using Variational Implicit Surfaces for Model Building. Technical Report KUL/ESAT/PSI/0601, Katholieke Universiteit Leuven, Belgium (January 2006).

Vannier, M.W., Gado, M.H., Marsh, J.L., 1983. Three-dimensional display of intracranial soft-tissue structures. American Journal of Neuroradiology 4 (3), 520–521.

Waters, K., 1992. A physical model of facial tissue and muscle articulation derived from computer tomography data. In: Proceedings of SPIE, vol. 1808, pp. 574–583.

Westermark, A., Zachow, S., Eppley, B., 2005. Three-dimensional osteotomy planning in maxillofacial surgery including soft tissue prediction. Journal of Craniofacial Surgery 16 (1), 100–104.

Zachow, S., Gladiline, E., Hege, H.-C., Deuflhard, P., 2000. Finite-element simulation of soft tissue deformation. In: Proceedings of CARS, pp. 23–28.

Zachow, S., Gladilin, E., Zeilhofer, H.-F., Sader, R., 2001. Improved 3D osteotomy planning in cranio-maxillofacial surgery. Lecture Notes in Computer Science (MICCAI) 2208, 473–481.

Zachow, S., Hierl, T., Erdmann, B., 2004. A quantitative evaluation of 3D soft tissue prediction in maxillofacial surgery planning. In: Proceedings of 3 Jahrestagung der Deautschen Gesellschaft für Computer- und Robotor-assistierte Chirurgie, Munchen, pp. 75–79.

Zienkiewicz, O.C., Taylor, R.L., 2000. The Finite Element Method: Volume 1 – The Basis, fifth ed. Butterworth Heinemann, London.